Published as: *Nature*. 2012 August 9; 488(7410): 172–177.

Deconstruction of a neural circuit for hunger

Deniz Atasoy, **J. Nicholas Betley**, **Helen H. Su**, and **Scott M. Sternson***
Janelia Farm Research Campus, HHMI, 19700 Helix Dr. Ashburn, VA 20147, USA

Abstract

Hunger is a complex behavioural state that elicits intense food seeking and consumption. These behaviours are rapidly recapitulated by activation of starvation-sensitive AGRP neurons, which present an entry point for reverse-engineering neural circuits for hunger. We mapped synaptic interactions of AGRP neurons with multiple cell populations and probed the contribution of these distinct circuits to feeding behaviour using optogenetic and pharmacogenetic techniques. An inhibitory circuit with paraventricular hypothalamus (PVH) neurons substantially accounted for acute AGRP neuron-evoked eating, whereas two other prominent circuits were insufficient. Within the PVH, we found that AGRP neurons target and inhibit oxytocin neurons, a small population that is selectively lost in Prader-Willi syndrome, a condition involving insatiable hunger. By developing strategies for evaluating molecularly-defined circuits, we show that AGRP neuron suppression of oxytocin neurons is critical for evoked feeding. These experiments reveal a new neural circuit that regulates hunger state and pathways associated with overeating disorders.

Hunger involves interoceptive sensory neurons that monitor metabolic signals and consequently regulate food seeking and consumption behaviours. To isolate discrete neural circuit pathways controlling feeding behaviour, we have focused on neurons in the hypothalamic arcuate nucleus (ARC) that express the gene *Agouti related protein* (*Agrp*). These are sensory neurons that are activated by circulating signals of energy deficit, such as ghrelin[1–3]. Elevated AGRP neuron electrical activity rapidly evokes voracious eating, even in well-fed mice[4,5]. Conversely, ablation of AGRP neurons results in aphagia[6], and suppressing their electrical activity lowers food intake[5]. Therefore, these molecularly-defined neurons that sense energetic need provide an entry point to neural circuits that mediate the "wisdom of the body"[7] and are sufficient to orchestrate complex counter-regulatory behavioural responses.

AGRP axon projections reveal an anatomical map[8] of brain regions that are potential downstream neuronal mediators of feeding behaviour (Supplementary Fig. 1). To establish pathways through which interoceptive sensory neurons acutely orchestrate feeding, we activated AGRP neurons while perturbing their output at downstream circuit nodes. We focused on three brain areas that receive AGRP neuron axonal inputs and also have an

*To whom correspondence should be addressed. sternsons@janelia.hhmi.org (S.M.S.), Phone: 571-209-4103, Fax: 571-209-4914.

Author Contributions D.A., J.N.B., and S.M.S. designed the experiments and analyzed data. D.A. and J.N.B. performed experiments. H.H.S. performed molecular cloning for viral constructs. S.M.S. and D.A. wrote the manuscript with comments from all of the authors.

established regulatory role in feeding behaviour: *Proopiomelanocortin* (*Pomc*)-expressing neurons in the ARC[4,9,10], parabrachial nucleus (PBN) neurons in the hindbrain[11,12], and paraventricular hypothalamus (PVH) neurons[13–15] (Supplementary Fig. 1). It is unclear which of these pathways mediate the dramatic short-term (<1 hour) feeding behaviours evoked by AGRP neuron activation.

We used optogenetic and pharmacogenetic tools to examine these complex, molecularly-defined feeding circuits in genetically modified mice. Our approach (Supplementary Fig. 2) involves first determining connectivity and synaptic properties between molecularly-defined neurons. We then investigated functional consequences of mapped synaptic connections by perturbing electrical activity in pre- and post-synaptic cell types both independently and in concert while monitoring the behavioural response. This is an experimental approach derived from the logic of classical epistasis analysis[16], used to order mutations into functional pathways or to establish the functional significance of protein interaction networks[17]. Here, we have extended this approach to neuronal activity perturbations in order to establish the functional significance of molecularly-defined neural circuits in behaving mice. Our results constrain existing circuit models and also reveal new circuit connections that are directly involved in mediating acute AGRP neuron-evoked feeding behaviour.

Results

Intra-ARC connectivity and function

We first considered the interaction of AGRP neurons in a local circuit with intermingled POMC neurons (Fig. 1a), a population that suppresses food intake[4,9]. In light of functional opposition between these neurons, their interaction has been implicated as a critical control point for feeding behaviour[18,19].

Channelrhodopsin-assisted circuit mapping[20] was used to precisely test the functional connectivity matrix of four possible direct synaptic interactions between these two populations (Supplementary Fig. 3a). $ARC^{AGRP}\rightarrow ARC^{POMC}$ connections were probed in *Agrp-Cre;Pomc-TopazFP* bi-transgenic mice in which AGRP neurons were rendered photoexcitable with channelrhodopsin-2[21] fused to tdTomato (ChR2:tdTomato), using a Cre recombinase (Cre)-dependent recombinant adeno-associated virus (rAAV)[22] (Fig. 1a,b). In brain slices, synaptic currents were recorded from POMC neurons while photostimulating AGRP neurons and their axons, which evoked reliable monosynaptic responses in all POMC neurons tested (n = 19) (Fig. 1b,c, Supplementary Fig. 4a–e). $ARC^{AGRP}\rightarrow ARC^{POMC}$ synapses exhibited paired-pulse depression, indicating high release probability (Supplementary Fig. 4f,g). Selective activation of $ARC^{AGRP}\rightarrow ARC^{POMC}$ synaptic connections strongly inhibited POMC neuron activity (Fig. 1d). This circuit connection was blocked by picrotoxin (PTX) (Fig. 1b), a $GABA_A$ (gamma-aminobutyric acid) receptor antagonist, showing that synaptic transmission and POMC neuron suppression required GABA and further indicating that other neuromodulatory substances released under these conditions are not sufficient to silence POMC neurons (Supplementary Fig. 3c). In contrast, no synaptic responses were observed for $ARC^{AGRP}\rightarrow ARC^{AGRP}$, A R $C^{POMC}\rightarrow ARC^{AGRP}$, or $ARC^{POMC}\rightarrow ARC^{POMC}$ (but see ref. 23) connections tested with other transgenic mouse line combinations (Fig. 1c, Supplementary Fig. 3, and Methods). Axon-attached

electrophysiological recordings confirmed that connection probability differences were not a consequence of axonal photoexcitability discrepancies (Supplementary Fig. 5). Thus, comprehensive dissection of connectivity in this molecularly-defined circuit reveals striking synaptic specificity.

To test acute behavioural consequences of the $ARC^{AGRP}\rightarrow ARC^{POMC}$ inhibitory connection, we first investigated the sufficiency of POMC neuron inhibition to influence feeding. Cre-dependent rAAV[22] was used to target the pharmacogenetic activity silencer hM4D[24] to POMC neurons in *Pomc-Cre* mice (POMC-hM4D mice; Fig. 1e). An hM4D agonist, clozapine-N-oxide (CNO, 10 μM), suppressed POMC neuron activity (Fig. 1f). However, intraperitoneal administration of CNO (5 mg/kg) to POMC-hM4D mice did not significantly alter food intake over 1 h (Fig. 1g, Supplementary Fig. 6a,b). Chronic POMC neuron suppression (24 h) did increase food intake, and this was dependent on efficient, bilateral transduction of POMC neurons (Supplementary Fig. 6c–e). Thus, POMC neuron suppression does not acutely activate feeding behaviour but does influence long-term food intake.

We also tested the possibility that POMC neuron inhibition might be required for AGRP neuron-evoked eating. A traditional approach, such as targeted injection of a $GABA_A$ receptor antagonist, is not cell type-specific and would release from inhibition all neurons at the injection site (Supplementary Fig. 2c). To overcome this lack of specificity, we developed a cell type-specific occlusion test to evaluate the behavioural necessity of inhibitory connections between molecularly-defined neuron populations by simultaneously co-activating AGRP and POMC neurons to surmount $ARC^{AGRP}\rightarrow ARC^{POMC}$ inhibition (Fig. 1h, Supplementary Fig. 2c).

AGRP and POMC neurons in *Agrp-Cre;Pomc-Cre* bi-transgenic mice were co-transduced with ChR2:tdtomato. We first determined that $ARC^{AGRP}\rightarrow ARC^{POMC}$ inhibitory input could be overcome by ChR2-mediated excitation in POMC neurons (Supplementary Fig. 7). In behavioural experiments, co-activation of AGRP and POMC neurons showed robust AGRP neuron-evoked feeding and rapid latency to eat, even with high ChR2 transduction efficiency in POMC neurons (Fig. 1i,j; Supplementary Fig. 7g,h). Therefore, suppression of POMC neuron activity by AGRP neurons is not required for acute feeding.

Long-range AGRP neural circuit function

We next considered long-range synaptic targets of AGRP neurons[8]. We focused on projections to the PVH in the hypothalamus and to the PBN in the hindbrain because PVH lesions lead to hyperphagia and obesity[13], while pharmacological inhibition in the PBN promotes feeding[25] and rescues aphagia induced by AGRP neuron ablation[11]. However, the relative role for these two projections in AGRP neuron-evoked feeding behaviour is uncertain. To directly examine these circuits, we used rapid cell type-specific activation of AGRP axons in the PVH and the PBN.

ChR2-expressing AGRP axons were stimulated with light pulses from an optical fibre placed above either the PVH or the PBN (Fig. 2a). Photoactivation of $ARC^{AGRP}\rightarrow PVH$ axons elicited food intake with similar magnitude as stimulating AGRP-expressing somata

in the ARC (Fig. 2b). Conversely, $ARC^{AGRP}\rightarrow$PBN axon activation did not significantly increase feeding (Fig. 2c,d). Moreover, for mice in which optical fibres were placed above both the PVH and the PBN, robust feeding was only evoked with illumination of the PVH, and there was no significant correlation ($r = 0.17$, $P = 0.68$) for food intake during photostimulation of these two brain areas (Supplementary Fig. 8a). We also observed that the proportion of AGRP-containing axons co-expressing ChR2:tdtomato diverged between the PBN and the PVH, with several rAAV-transduced mice showing ChR2-penetrance biased to the PVH (Supplementary Fig. 8b and see Methods). The dissociation of ChR2-penetrance in AGRP axons between these two brain regions was also apparent from linear regression analysis ($r = 0.83$, $P = 0.006$; y-intercept > 0, $P = 0.01$, Supplementary Fig. 8b), indicating that not all PVH-projecting AGRP neurons also project to the PBN. Moreover, $ARC^{AGRP}\rightarrow$PVH activation evoked feeding in mice with modest ChR2-penetrance to AGRP axons, while $ARC^{AGRP}\rightarrow$PBN evoked feeding was not clearly evident even with high ChR2-penetrance (Supplementary Fig. 8c). Therefore, activation of axons in and around the PVH is substantially more effective than those in the PBN for acute, AGRP neuron-mediated induction of feeding behaviour. In light of these findings, we investigated $ARC^{AGRP}\rightarrow$PVH circuit properties and their relationship to food seeking and consumption behaviour.

$ARC^{AGRP}\rightarrow$PVH synapse properties

Feeding evoked by activation of AGRP axons in the PVH does not conclusively demonstrate that the PVH is the downstream target. This behavioural effect may also involve activation of AGRP neuron axons-of-passage and antidromic action potentials that could activate AGRP neuron projections to other brain regions. To address this, we investigated AGRP neural circuit connections in the PVH.

We first determined whether AGRP axons in the PVH made synapses that could influence PVH neuronal function. Immunohistochemical analysis revealed AGRP-containing synaptic release sites in the PVH (Supplementary Fig. 9a). Functional synaptic connectivity was measured with channelrhodopsin-assisted circuit mapping[20] in the PVH. Photostimulation of AGRP axons evoked synaptic currents in PVH neurons (29/61 cells, 48%). These responses were blocked by PTX (9/9 cells), indicating that they were mediated by GABA (Fig. 3a).

GABA-releasing synapses can exhibit specializations that are essential to their circuit function[26,27]. Optogenetic methods were used to characterize $ARC^{AGRP}\rightarrow$PVH synaptic connections. The most prominent synaptic characteristic was a barrage of delayed asynchronous inhibitory postsynaptic currents (IPSCs) that continued for up to 1 s following AGRP axon stimulation by a single 1 ms light pulse (Fig. 3b). This property was also observed in other AGRP neuron projection targets (Fig. 1b, Supplementary Fig. 10). These experiments were performed with glutamate receptor antagonists to minimise possible network interactions, and multiple lines of evidence demonstrate that asynchronous release is not a result of photostimulation artefacts (Supplementary Fig. 9). Moreover, axon-attached recordings show that each photostimulus elicits only one axonal action potential (Supplementary Fig. 5).

Asynchronous release increased during repetitive stimulation of $ARC^{AGRP}\rightarrow PVH$ projections and synapses quickly developed a slow (DC) component[27] that did not return to baseline between the optical stimuli (Fig. 3c,d). Moreover, GABA continued to be released following the stimulus train, and the final IPSC decayed nearly 30-fold more slowly than the underlying $ARC^{AGRP}\rightarrow PVH$ quantal IPSCs (Fig. 3e and Methods), which corresponded to a large increase in charge transfer to the postsynaptic neuron after the evoked synchronous IPSC of the last photostimulus (Fig. 3f). Both aspects of asynchronous release were significantly reduced with the membrane-permeable calcium buffer, EGTA-AM (100 μM), indicating that accumulation of free calcium in the synaptic terminal contributes to this property (Fig. 3e,f).

Prolonged asynchronous GABA release at $ARC^{AGRP}\rightarrow PVH$ synapses reduced both spontaneous (Fig. 3g) and evoked (Supplementary Fig. 11) PVH excitability for hundreds of milliseconds following IPSCs, a timescale often associated with neuromodulation, but mediated here solely by action at ionotropic GABA receptors (Fig. 3g and Supplementary Fig. 11d). This property confers strong inhibition to these synapses, which can influence postsynaptic activity for hundreds of times longer than each AGRP neuron action potential.

Sufficiency and necessity of $ARC^{AGRP}\rightarrow PVH$

Multiple observations suggest that AGRP neurons increase feeding, in part, by inhibiting neurons in the PVH: $ARC^{AGRP}\rightarrow PVH$ synaptic connections are specialised to strongly inhibit postsynaptic targets (Fig. 3); this projection is associated with AGRP neuron-evoked eating (Fig. 2); and we have found that food deprivation increases inhibitory synaptic drive onto PVH neurons (Supplementary Fig. 12). Also, $GABA_A$ receptor agonist injections around the ventral thalamus and medial hypothalamus lead to eating[28]. Therefore, we investigated the causal relationship between feeding behaviour and selective PVH neuron inhibition.

The gene *Sim1* is expressed with regional selectivity in nearly all PVH neurons[29]. We used *Sim1-Cre* transgenic mice to target the neuronal silencer, hM4D, to neurons in the PVH (SIM1-hM4D mice, Fig. 4a). CNO significantly suppressed SIM1 neuron electrical activity (Supplementary Fig. 13a,b). In SIM1-hM4D mice, CNO increased food intake (Fig. 4b,c and Supplementary Fig. 13c), similar to AGRP neuron photostimulation[4] and in marked contrast to POMC neuron silencing (Fig. 1g).

Since hM4D acts through a G_i-coupled signalling pathway, the effect on feeding might not be a direct result of neuronal inhibition. Therefore, we used an alternative pharmacologically selective neuronal silencer system which can effectively mimic prolonged ionotropic GABA receptor activation by directly increasing chloride conductance[30]. Silencing SIM1 neurons with $PSAM^{L141F}$-GlyR chimeric ion channels and a cognate selective ligand ($PSEM^{308}$) also rapidly evoked feeding (Supplementary Fig. 13d,e). Both of these experiments are consistent with acute PVH inhibition as an important contributor to AGRP neuron-evoked feeding behaviour.

Deprivation-induced hunger and AGRP neuron activation are both associated with an increased willingness to work for food[5,31]. To explore whether AGRP neural circuits could

be used to identify new motivationally-sensitive brain regions, we also compared the motivational shift induced by AGRP neuron activation, SIM1 neuron silencing, and food deprivation in an instrumental lever press task. We used progressive ratio (PR) food pellet reinforcement, where the highest reinforcement schedule attained is termed the break point, a measure of motivation[31]. Well-fed AGRP-ChR2 and SIM1-hM4D mice both increased break point during either AGRP neuron activation or SIM1 neuron silencing (Fig. 4d) but not in control mice (Supplementary Fig. 13f). Together, these results show that both food seeking and food consumption responses to AGRP neuron activation are replicated by suppressing the electrical activity of SIM1 neurons. Moreover, circuit mapping approaches allowed us to identify the PVH, which has not been previously implicated in instrumental responses for reinforcement, as a motivationally important brain region.

We also tested the necessity of this circuit connection for elevated food intake using co-activation of SIM1 neurons to selectively overcome $ARC^{AGRP}\rightarrow PVH$ inhibition (Fig. 4e). In PVH-containing brain slices from *Agrp-Cre;Sim1-Cre* bi-transgenic mice where both neuron populations were virally transduced to express ChR2, we determined that co-stimulation of SIM1 neurons along with AGRP axons overcame the inhibitory response from $ARC^{AGRP}\rightarrow PVH$ projections (Supplementary Fig. 13h). *In vivo*, co-stimulation of $ARC^{AGRP}\rightarrow PVH$ projections and SIM1 neurons, completely suppressed AGRP neuron-evoked eating (Fig. 4f). *Post hoc* analysis showed that AGRP neurons were still activated under these conditions (Fos+/ChR2+: 77 ± 2%, $n = 3$). Thus, PVH inhibition is both necessary and sufficient for acute feeding evoked by $ARC^{AGRP}\rightarrow PVH$ axon projections.

$ARC^{AGRP}\rightarrow PVH^{OXT}$ connectivity and function

The PVH is a heterogeneous brain structure with different cell types[32,33]. Within the PVH, oxytocin (OXT) neuron loss-of-function is implicated in Prader-Willi syndrome[34] and also as a consequence of *SIM1* mutations[29,35,36], both of which are associated with overeating and obesity in people. To refine $ARC^{AGRP}\rightarrow PVH$ connectivity, we investigated OXT neurons as potential postsynaptic targets of this inhibitory projection.

Functional circuit mapping experiments showed that OXT neurons, a small subpopulation of PVH neurons[33] identified in *Agrp-Cre;Oxytocin-Gfp* bi-transgenic mice, exhibited substantially higher connection probability with AGRP neurons (12/17 cells, 71%) than for neighbouring unlabeled neurons (6/18 cells, 33%; Supplementary Fig. 14a–c). Despite its prominence, this $ARC^{AGRP}\rightarrow PVH^{OXT}$ connection has not been previously described, in part due to the difficulty of conclusively demonstrating cell type-specific synaptic connections without optogenetic electrophysiological methods. In addition, the $ARC^{AGRP}\rightarrow PVH^{OXT}$ circuit was strongly inhibitory (Supplementary Fig. 14d), therefore AGRP neurons may activate feeding through inhibition of OXT neurons.

We tested the behavioural necessity of this circuit by occlusion of synaptic inhibition at this molecularly-defined circuit connection with co-activation of OXT neurons and AGRP neuron projections. OXT neurons were rendered photoexcitable by transduction with rAAV expressing ChR2:tdTomato from an *Oxytocin* promoter fragment[37,38] (Supplementary Fig. 14e–h), and *in vivo* photostimulation increased Fos expression selectively in OXT neurons

(Supplementary Fig. 14i,j). Photostimulation over the PVH containing both ChR2-expressing OXT neurons and AGRP axons strongly suppressed evoked feeding (Fig. 5a,b).

To confirm that suppression of feeding was dependent on $ARC^{AGRP}\rightarrow PVH^{OXT}$ circuit connectivity and not an autonomous OXT neuron pathway, we used a cell type-specific circuit disconnection strategy. Because $ARC^{AGRP}\rightarrow PVH$ projections are lateralised (~3:1 ipsilateral:contralateral projection bias), we stimulated unilaterally transduced OXT neurons either ipsilateral or contralateral to the side of unilateral AGRP neuron transduction (Fig. 5c). Ipsilateral OXT neuron stimulation significantly suppressed $ARC^{AGRP}\rightarrow PVH$ stimulation-induced feeding and contralateral OXT neuron stimulation did not (Fig. 5d,e, Supplementary Fig. 14k). Occlusion of the ipsilateral $ARC^{AGRP}\rightarrow PVH^{OXT}$ circuit is likely an underestimate because $ARC^{AGRP}\rightarrow PVH$ projections are not strictly ipsilateral. Notably, bilateral stimulation of OXT neurons alone in food-deprived mice during re-feeding, which is mediated by multiple cell types and circuits, did not significantly reduce consumption (Supplementary Fig. 14l), thus the anorexigenic effect of OXT neuron activation is most apparent during selective activation of AGRP axons in the PVH. All together, these experiments identify the molecularly-defined circuit projection $ARC^{AGRP}\rightarrow PVH^{OXT}$ as a synaptic pathway for AGRP neurons in the PVH and demonstrate an important role for this connection in AGRP neuron-evoked eating.

Pharmacologic analysis of evoked feeding

A remaining question concerns the relative behavioural contribution of GABA and neuropeptides released by AGRP neurons. We previously showed that the neuromodulator Agrp was not necessary for acute feeding behaviour[4], but a role for co-released Npy is possible because this peptide potently activates feeding when injected to the PVH[39]. Initial circuit characterization experiments using $Npy^{-/-}$ mice to address the necessity of Npy release showed dramatic strengthening of GABA signalling in $ARC^{AGRP}\rightarrow PVH$ circuitry (connectivity rate, *Agrp-Cre*: 48%, *Agrp-Cre;*$Npy^{-/-}$: 69%; paired-pulse ratio, *Agrp-Cre*: 0.81 ± 0.08, $n = 24$; *Agrp-Cre;*$Npy^{-/-}$: 0.46 ± 0.09, $n = 28$; $P = 0.01$, unpaired *t*-test), likely due to substantial developmental compensation in these circuits. Therefore, to probe the contribution of these transmitters to $ARC^{AGRP}\rightarrow PVH$ neuron-evoked food intake while minimizing compensatory effects, we pharmacologically blocked $GABA_A$ receptors and Npy1r in the PVH during $ARC^{AGRP}\rightarrow PVH$ axon activation. Blockade of either receptor strongly inhibited evoked food intake during $ARC^{AGRP}\rightarrow PVH$ photostimulation (Fig. 6a,b), indicating that concerted signalling through both receptor types was essential for the behavioural effects of AGRP axon activation in the PVH.

Robust pharmacological suppression of feeding in the $ARC^{AGRP}\rightarrow PVH$ circuit allowed us to use pharmacology to examine the overall necessity of this projection pathway in the context of somatic AGRP neuron-evoked eating, which is expected to activate all AGRP neuron circuit projections. For this, we activated AGRP neurons, using the pharmacogenetic activator hM3D with its ligand CNO[5,24], and blocked either GABA or Npy signalling in the PVH (Fig. 6c). $GABA_A$ or Npy1r antagonists in the PVH significantly reduced food intake during AGRP neuron activation (Fig. 6d). These results indicate that, even with brain-wide activation of AGRP neural circuits, signalling in the PVH is critical and involves both

$GABA_A$ and Npy receptors. Strikingly, though, in these experiments, and in contrast to $ARC^{AGRP}\rightarrow$PVH projection activation, feeding remained significantly above baseline (Fig. 6d). Thus, while our results show that AGRP neuron-evoked eating is mediated, in part, by the PVH, there are additional behaviourally important circuits awaiting further investigation.

Discussion

Hunger is mediated by neural circuits that integrate visceral signals of energetic state and consequently regulate physiology and behaviour. Applying optogenetic circuit mapping, we determined functional connectivity from starvation-sensitive AGRP neurons to synaptic targets with cell type-specific precision and then evaluated the functional significance of these connections for feeding behaviour by manipulating the circuit nodes independently or together in behaving mice (Supplementary Fig. 15a). Based on these experiments and the results of others, three distinct functions can be assigned to anatomically separate projection fields of AGRP neurons (Supplementary Fig. 15b). 1) We show directly that AGRP neurons strongly inhibit POMC neurons, which do not acutely regulate feeding behaviour. However, cell type-specific activation[4] and silencing experiments indicate that they likely regulate longer-term feeding responses. 2) We find prolonged inhibition of PVH neurons by synapses from AGRP axons. Suppression of PVH neurons is sufficient for acute AGRP neuron-evoked eating, which also includes the motivational consequences of AGRP neuron activation. In addition, the $ARC^{AGRP}\rightarrow$PVH circuit projection is necessary for a significant portion of AGRP neuron-evoked eating; however other brain regions likely contribute. 3) Finally, AGRP neuron projections targeting the parabrachial nucleus (PBN) in the hindbrain do not directly activate feeding, but instead they restrain visceral malaise that results from AGRP neuron ablation[11]. Future experiments could investigate the possibility that this is due to separate AGRP neuron subpopulations in the ARC with different axonal projection patterns. In any event, multiple mechanisms involved in hunger are dissociated into distinct behavioural modules by anatomically separate AGRP neuron axonal projections

These experiments also support an important link between forebrain and hindbrain control of feeding behaviour. In the forebrain, we have identified OXT neurons as a key target of AGRP neurons for controlling acute feeding behaviour. OXT potently suppresses feeding when delivered to the brain but not the periphery[40], thus non-neuroendocrine OXT neurons, which project to the hindbrain and spinal cord[33,41], likely mediate these anorexigenic effects. Oxytocin signalling enhances hindbrain responses to circulating satiety signals[42], and genetic disruption of synaptic release from OXT neurons[43] or ablation of OXT receptor-expressing hindbrain neurons both lead to overeating[44]. Loss of OXT neurons is also associated with both Prader-Willi syndrome and *SIM1* mutations, each of which lead to insatiable hunger in people, presumably due to a disrupted satiety response[29,34–36]. These experiments define a circuit for voracious AGRP neuron-evoked eating and link these neurons that regulate energy homeostasis to hindbrain-projecting neurons involved with human genetic conditions that lead to remarkably similar characteristics to the evoked behaviour: profound hunger, motivation for food, and resultant obesity. This mechanistic relationship implies that AGRP neuron activation may be a behavioural model that could be used to explore therapeutic approaches to overeating observed in these conditions. Further investigation into the “hunger modules” described here using cell type-specific mapping and

manipulation techniques will permit elaboration of this circuit framework for feeding regulation and provide insight into this behaviour under healthy conditions and in association with overeating disorders.

METHODS

All experimental protocols were conducted according to U.S. National Institutes of Health guidelines for animal research and were approved by the Institutional Animal Care and Use Committee at Janelia Farm Research Campus.

Mice

Animals were housed on a 12 hour light (06:00)/dark (18:00) cycle with *ad libitum* access to water and mouse chow (PicoLab Rodent Diet 20, 5053 tablet, TestDiet), unless otherwise noted. *Agrp-Cre*[45], *Agrp-IRES-Cre*[19], *Pomc-Cre*[46], *Sim1-Cre*[14], *Oxytocin-Gfp*[47], *Pomc-TopazFP*[48], *NPY-SapphireFP*[48], *Npy*$^{-/-}$[49] mice have been described previously. In most cases, behavioural experiments were with male mice. Females were used for some SIM1 neuron silencing experiments (6/19, Fig. 4). Most experiments used *Agrp-Cre*[45] mice, except experiments in Figs. 2b (subset), 2c–g, 6, which were performed with *Agrp-IRES-Cre*[19] mice.

Viral vectors

rAAV2/1-*CAG*-FLEX-*rev*-ChR2:tdTomato was described previously[22]. The rAAV-*CAG*-FLEX-hM4D:2a:GFP vector was prepared by ligating hM4D and EGFP with an intervening DNA fragment for a 2a peptide from Porcine teschovirus (GSGATNFSLLKQAGDVEENPGP), which was inserted into the rAAV2-*CAG*-FLEX backbone in an inverted orientation. rAAV2/1-*hSyn*-FLEX-*rev*-hM3D:mCherry was from the UNC viral core facility. For rAAV2-*Oxytocin*-ChR2:tdTomato, we used a mouse *Oxytocin* promoter fragment (−600 to −1, forward: 5′-CAAGGCCAGCCTGGTCTACACAGCAGG-3′, reverse: 5′-GGCGATGGTGCTCAGTCTGAGATCCGC-3′), followed by the Promega chimeric intron and ChR2:tdTomato, which were ligated into an rAAV2 backbone. Viral vectors were produced by the University of Pennsylvania Gene Therapy Program Vector Core or the Janelia Farm Molecular Biology Core Facility.

Viral injections and fibre placement

Viral injections were performed as described previously[22] (P21 – P25 for electrophysiological recordings, P40 –P50 for behavioural experiments). ARC coordinates: bregma −1.2 mm, midline +0.2 mm; dorsal surface −5.85 mm and −5.75mm. PVH coordinates: bregma −0.7 mm; midline ±0.3 mm; dorsal surface −4.5 mm and −4.3 mm. For behavioural experiments that required photostimulation, a guide cannula was inserted (ARC: 4.5 mm, 26GA; PVH: 3.5 mm, 26GA). For PVH^{OXT} neuronal activation, cannula placement was through a midline craniotomy. For PBN/PVH photostimulation in the same mouse, adult male *Agrp-IRES-Cre*[19] animals were bilaterally transduced in the arcuate nucleus with rAAV2/1-*CAG*-FLEX-*rev*-ChR2:tdTomato (600 nL). Ferrule-capped fibres (see below)

were implanted over the PVH (bregma: −0.7 mm, midline: +0.3 mm; dorsal surface: −4.0 mm) and PBN (bregma: −5.8 mm, midline: +0.9 mm; dorsal surface: −2.75 mm).

Grip cement (DENTSPLY) was used to anchor the guide cannula or ferrule-capped fibres to the skull. When needed, a dummy cannula (33GA, Plastics One) was inserted to keep the fibre guide from getting clogged. Postoperative analgesia was provided (ketoprofen, 5 mg/kg). After surgery, mice were allowed 14 – 20 d for recovery and transgene expression.

Pharmacology

Antagonists: $GABA_A$ (picrotoxin, 50 μM, Sigma), $GABA_B$ (saclofen, 50 μM, Tocris), ionotropic glutamate receptors (AP-5, 50 μM; CNQX, 10 μM; Sigma), Npy1r (PD160170, 1 μM, Tocris), Npy2r (BIEE 0246, 0.5 μM, Tocris), and Npy5r (CGP 71683, 10 μM, Tocris), voltage-gated sodium channels (tetrodotoxin, TTX, 1 μM, Sigma). Saclofen was included to prevent potential metabotropic $GABA_B$ receptor-mediated modulation of the postsynaptic neuron. Agonist: CNO (10 μM, BioMol). Pharmacological agents were bath applied with gravity perfusion.

Electrophysiology and circuit mapping

Experimental techniques were similar to those reported previously[22]. Detailed conditions for circuit mapping experiments in brain slices are in Table S1. Coronal brain slices were prepared in chilled cutting solution containing (in mM): 234 sucrose, 28 $NaHCO_3$, 7 dextrose, 2.5 KCl, 7 $MgCl_2$, 0.5 $CaCl_2$, 1 sodium ascorbate, 3 sodium pyruvate and 1.25 mM NaH_2PO_4, aerated with 95% O_2/5% CO_2. Slices were transferred to artificial cerebrospinal fluid (aCSF) containing (in mM): 119 NaCl, 25 $NaHCO_3$, 11 D-glucose, 2.5 KCl, 1.25 $MgCl_2$, 2 $CaCl_2$ and 1.25 NaH_2PO_4, aerated with 95% O_2/5% CO_2. Slices were incubated at 34 °C (30 min) and then maintained and recorded from at room temperature (20 – 24 °C). The intracellular solution for voltage clamp recordings contained (in mM): 125 CsCl, 5 NaCl, 10 HEPES, 0.6 EGTA, 4 Mg-ATP, 0.3 Na_2GTP, 10 lidocaine *N*-ethyl bromide (QX-314), pH 7.35 and 290 mOsm/L. The holding potential for voltage clamp recordings was −60 mV unless otherwise indicated. The intracellular solution for current clamp recordings contained (in mM): 125 potassium gluconate, 6.7 KCl, 10 HEPES, 1 EGTA, 4 Mg-ATP, 10 sodium phosphocreatine (pH 7.25; 290 mOsm/L), E_{Cl} = −75 mV. In a subset of experiments potassium gluconate-based internal solution was used for voltage clamp recordings. In most intracellular recordings, internal solutions contained GDP-βS (0.5 mM, Sigma).

For brain slice photostimulation, a laser (473 nm) was used to deliver light pulses ranging from 0.1 – 1 mW at the specimen. Laser power was monitored with a photodiode for each light pulse. Light pulse duration (1 ms) was controlled by a Pockels cell (ConOptics) and a mechanical shutter (Vincent Associates). A focal spot was targeted onto the specimen with two scanning mirrors (Cambridge Technology) through 4× or 63× objectives.

For electrical stimulation, a field electrode was placed within the ARC (for measurements from ARC) or adjacent tothe third ventricle to activate the ascending fibre tract (for

measurements from the PVH). Half-maximal stimulus strength was used for asynchronous release or paired-pulse ratio measurements.

Loose-seal, cell-attached recordings (seal resistance, 20–70 MΩ, aCSF internal) were made in voltage clamp with holding current maintained at zero. Most neurons fired spontaneously. For measuring $ARC^{AGRP}\rightarrow ARC^{POMC}$ and $ARC^{AGRP}\rightarrow PVH^{OXT}$ influence on spontaneous firing rate, the postsynaptic neurons were recorded while ChR2-expressing axons were photostimulated in the absence of any blockers (Supplementary Fig. 3c, Supplementary Fig. 14d) or in the presence of Npy1r, Npy5r, and $GABA_B$ receptor blockers (Fig. 1d, Fig. 3g). hM4D-dependent neuronal silencing was tested in POMC and SIM1 neurons in the presence of glutamate and $GABA_A$ receptor blockers.

For axon-attached recordings, an aCSF-filled recording electrode (8 – 10 MΩ) was used, and ionotropic glutamate and $GABA_A$ receptors were blocked. After a subset of recordings, TTX (1 μM) was used to confirm that signals were due to action potentials. AGRP or POMC axons in the PVH were identified and targeted by tdTomato fluorescence.

For asynchronous release measurements, CNQX, AP5 and saclofen were present. Asynchronous release was also prominent in the absence of saclofen (Fig. 1b, Fig. 3b). For analysis of asynchronous release, traces from 8–10 trials were averaged. The DC component during photostimulation was calculated by measuring the current amplitude 2 ms before each photostimulus and was normalised to the peak amplitude of the first synchronous synaptic response (Fig. 3d). Decay times for the delayed asynchronous component in the train stimulus were calculated by a single exponential fit starting 100 ms following last light pulse (Fig. 3e). Cumulative charge from delayed release was calculated as the total area under the averaged traces 100 ms – 3 s following last pulse (Fig. 3f). For baseline charge transfer a 3 s pre-stimulus window was used.

Quantal amplitude measurements (Fig. 3e) were performed under the same conditions as above except that, in the aCSF, 2 mM Ca^{2+} was replaced by 2 mM Sr^{2+}. Quantal events were chosen from a window immediately following stimulation until the event frequency dropped to three times above the baseline spontaneous event frequency.

In vivo photostimulation

Components for food consumption monitoring and photostimulation were similar to those reported previously[4]. Light was delivered to the brain through an optical fibre (200 μm diameter core; BFH48–200-Multimode, NA 0.48; Thorlabs), which was implanted through the fibre guide the day before photostimulation. The fibre tip was positioned to a distance of ~0.8 mm from the targeted region. The relationship of light scattering and absorption in the brain as a function of distance has been described previously[50]. Using this relationship, the light power exiting the fibre tip (10 – 15 mW) was estimated to correspond to >2.0 mW mm^2 at the ARC or PVH. For optical delivery of light pulses with millisecond precision to multiple mice, the output from a diode laser (473 nm, Altechna) was split into eight beams using a combination of 50/50 beam splitters and turning mirrors (Thorlabs). The main output beam from the diode laser was controlled using an acousto-optic modulator (AOM) (Quanta Tech, OPTO-ELECTRONIC) to generate light pulses that were launched into separate fibre

ports (PAF-X-5 or PAF-X-7, Thorlabs) and their corresponding optical fibres. Using these components, eight mice could be simultaneously photostimulated. For all *in vivo* photostimulation experiments the same pulse protocol was used: 10 ms pulses, 20 pulses for 1 s, repeated every 4 s for 1 h.

For $ARC^{AGRP}\rightarrow PVH^{OXT}$ photostimulation experiments in which ipsilateral and contralateral sides were dissociated (Fig. 5), mice with missed injections, bilateral injections (either in ARC or PVH) or low Fos expression in AGRP neurons were excluded.

For bilateral OXT neuron photostimulation following food deprivation, (Supplementary Fig. 14l) experiments were performed in mice bilaterally infected with rAAV2/1-*Oxytocin*-ChR2-tdTomato that were food deprived for 24 hours. Before re-feeding (5 min), photostimulation was initiated through a cannula placed over the PVH midline. Mice were allowed *ad libitum* access to food for 2 days after which OXT neurons were photostimulated again for 1 hour. Immediately following photostimulation, mice were perfused and their brains were fixed, sectioned, and stained for Oxt- and Fos-immunoreactivity (Supplementary Fig. 14i).

For experiments in which $ARC^{AGRP}\rightarrow PVH$ and $ARC^{AGRP}\rightarrow PBN$ projection stimulation were in the same animal, fibres were capped with 1.25 mm OD zirconia ferrules (see http://syntheticneurobiology.org/protocols/protocoldetail/35/9), implanted into the brain, and affixed to the skull of the animal with dental cement. For light delivery, the implanted ferrule-capped fibre was coupled to another optical fibre with a matching 1.25 mm OD zirconium ferrule using a zirconium sleeve.

Pharmacology of AGRP neuron evoked feeding

Surgeries and photostimulation were similar to $ARC^{AGRP}\rightarrow PVH$ stimulation experiments as described above except that cannula placement over the PVH was 0.25 mm lateral to the midline with other coordinates being the same. Prior to photostimulation (−10 min), vehicle [0.15 M saline, DMSO (10%), glacial acetic acid (2.5%)], Npy1r antagonist (BIBO-3304, 3 μg, Tocris), or $GABA_A$ receptor antagonist (bicuculline methiodide, 2.5 pmol, Sigma) were delivered on separate days through the same cannula that was used for fibre implantation. Antagonist injections were on the second or third day, counterbalanced between groups. Injections (50 nL) were through an injection cannula (33 Gauge) coupled to a Hamilton syringe that was driven by a Narishige micromanipulator (~30 nL/minute). Animals were subsequently photostimulated (1 h). Two animals had cannula blockage on the final day of injection (condition: bicuculline methiodide followed by photostimulation) and were eliminated from this analysis group.

PVH pharmacology experiments with the hM3D neuronal activator were performed as above, except that, instead of light delivery, mice were injected with CNO (intraperitoneal, 0.3 mg/kg, also see below) immediately prior to intracranial antagonist injection.

In separate mice, the effective concentration of BIBO-3304 was determined by the ability to block food intake evoked by Npy (70 pmol, Sigma) injection into the PVH. Consistent with earlier reports[51], Npy-dependent food intake was suppressed. We further confirmed that this

concentration does not induce a nonspecific inhibition of overall feeding response, by delivering the same dose into the PVH of 24 hour food deprived animals. While 3 μg BIBO-3304 effectively blocked Npy-induced food intake, it did not significantly decrease re-feeding after deprivation, although there was a trend for reduced food intake (Supplementary Fig. 16).

Neuron silencing

For hM4D-dependent silencing experiments, rAAV2/1-*CAG*-FLEX-*rev*-hM4D:2a:GFP virus injections were made bilaterally. Mice with total misses or unilateral injections were excluded from analysis after *post hoc* examination of GFP expression. CNO (5 or 0.3 mg/kg) or saline was delivered by intraperitoneal injection. Control saline injections contained an equivalent amount of DMSO (0.6%). Consistent with a previous report[5], we found that CNO injection alone did not stimulate food intake in uninfected mice (data not shown).

For $PSAM^{L141F}$-GlyR silencing experiments in SIM1 neurons, we bilaterally transduced *Sim1-Cre* mice with rAAV-*Synapsin*-FLEX-*rev*-$PSAM^{L141F}$GlyR:IRES:EGFP as described above for hM4D transduction of the PVH. A cognate ligand for this chimeric chloride channel, $PSEM^{308}$ (5 mg/kg) was dissolved in saline and administered intraperitoneally. Food intake was measured before (Pre) and after $PSEM^{308}$ administration (1 h each). $PSEM^{308}$ (5 mg/kg) was also administered to untransduced control mice.

Progressive ratio task

For the entire training protocol, all animals were maintained under *ad libitum* fed conditions, and were never pre-exposed to food deprivation or neuronal manipulation before the days on which these were tested. *Agrp-Cre* or *Sim1-Cre* mice were first acclimated to handling and were exposed to the testing arena in 3 sessions, where they became familiar with the pellet delivery system and food retrieval. To continue training, each animal had to consume at least 5 pellets from the food hopper on the last session. Animals were then trained to perform lever pressing for food pellets.

The response lever was placed adjacent to the food delivery cup. Animals were allowed one hour in the arena to perform Fixed Ratio (FR)1, FR3, and FR5, each for 3 days. After 5 training sessions, animals that were not pressing a lever sufficiently to earn at least 3 food pellets, were eliminated from further training and testing. To test whether lever pressing was reinforcer-directed, a second identical but inactive lever was placed in the arena on the opposite side of the food delivery cup on the third FR3 session. In successive training and experimental sessions, the inactive lever was rarely pressed as it never led to a food reinforcer.

For AGRP neuron activation experiments, break point testing was performed on a progressive ratio-2 schedule, such that each successive food reward increased the lever-press schedule by two additional responses. Break point is defined here as the lever-press schedule reached at the end of the one hour session[52]. The following day, an optical fibre was inserted into the guide cannula. The animal was allowed 1 hour in its home cage to habituate after

handling. After transfer to the behavioural test cage, the progressive ratio schedule was repeated in the *ad libitum* fed animal with photostimulation. The following day, food was removed from the home cage (24 h) with water freely available, followed by a break point test under food deprived conditions. After allowing at least 3 days for *ad libitum* repletion, the break point was tested again.

Progressive ratio experiments for SIM1 neuron silencing were performed similarly, except that each test session was extended to 2 hours due temporal variability for pharmacogenetic experiments following intraperitoneal injection. Due to the increased session length, a PR3 schedule was used to prevent satiation. Mice received saline injections in each test session except the day in which behavioural effect of SIM1 neuron silencing was tested. On that day they received a single dose of CNO (5 mg/kg, IP) immediately before being placed in the test cage. The experimenter was blind to the ChR2 or hM4D expression of the subjects, which was revealed after *post hoc* histology.

Image analysis of PVH-selectivity for SIM1 neuron transduction with hM4D was in Image-J. Confocal images across the rostro-caudal axis, included the PVH as well as neighbouring structures (1.3 mm × 1.3 mm), were subjected to the automated thresholding function, and total thresholded surface area was measured. Fluorescence within and outside of the PVH was calculated (n = 6 mice). hM4D-transduced SIM1 neurons were primarily located within the PVH (84 ± 2% of total fluorescence, n = 6 mice), and there was a negative correlation between break point and the small proportion of scattered hM4D-expressing neurons that extended outside the PVH (r = −0.7, Supplementary Fig. 13g).

Antibodies

anti-Agrp (1:5000, goat, Neuronomics), anti-Agrp (1:2000, rat, Neuronomics), anti-Fos (1:5000, rabbit, Santa Cruz), anti-αMSH (1:500, sheep, Millipore), anti-Pomc (1:200, rabbit, Phoenix Pharmaceuticals), anti-Oxytocin (1:3000, mouse, Abcam), anti-Synapsin I (1:1000, rabbit, Millipore), anti-tdTomato (1:20000, guinea pig, Covance), anti vGat (1:2000, rabbit, SySy). Fluorophore-conjugated secondary antibodies were from Invitrogen and Jackson Immuno. Antibodies were diluted in phosphate buffered saline, 1% BSA, 0.1% Triton X-100.

Immunohistochemistry and imaging

After mice were used for behavioural experiments, they were transcardially perfused with 4% paraformaldehyde/0.1 M phosphate buffer fixative. Tissue was post-fixed in this solution for 4 – 5 hours and washed overnight in phosphate buffered saline (pH 7.4). Brain sections (50 μm) were processed for immunohistochemistry, mounted on glass slides using VECTASHIELD mounting medium with 4′,6-diamidino-2-phenylindole (DAPI), and coverslipped for imaging.

Photostimulation experiments were confirmed by *post hoc* Fos quantification. After experiments were complete, mice were photostimulated (1 h) in the absence of food and immediately processed for perfusion, followed by sectioning as described above. Transduction of AGRP, SIM1 or OXT neurons was evaluated by the expression of ChR2-

tdtomato. After anti-Fos immunohistochemistry, nuclei were stained with DAPI, and confocal images (2 μm thickness, 5 images) were collected using a 20× (0.8 N.A.) objective, and ChR2 neurons were counted in a single section at the centre of the stack (stacks above and below were also examined to minimise false-negative reporting of Fos expression). Only cells that clearly had a nucleus demarcated by the presence of DAPI staining and surrounded by membrane-localised ChR2-tdtomato fluorescence were included. A subset of those neurons also had Fos-immunoreactivity overlapping with DAPI, and these neurons were taken as Fos-positive ChR2 neurons. Large DAPI-positive nuclei without any surrounding tdtomato fluorescence were considered ChR2-negative neurons. For each mouse, Fos-positive counts from three sections were averaged across the rostral-caudal axis of the ARC or PVH.

Axonal ChR2-penetrance

To quantify axonal ChR2-penetrance for PVH/PBN stimulation experiments, brain slices were immunostained for tdTomato to enhance detection, and confocal images were collected. The percentage of AGRP-containing varicosities transduced with ChR2:tdtomato in the PVH and the PBN were calculated using automated varicosity-detection in Vaa3D[53] (confirmed by manual inspection). At least 300 varicosities from three distinct sections along the rostral-caudal axis of the PVH and the PBN were analysed from each animal.

Statistics

Values are represented as means ± s.e.m. *P* values for pair-wise comparisons were calculated by two-tailed Student's *t*-test. *P* values for comparisons across more than two groups were adjusted with the Holm-Sidak correction. Linear regressions and tests involving 1-way and 2-way ANOVA with one factor repetition were calculated with SigmaPlot (Systat). n.s. $P > 0.05$, $*P < 0.05$, $**P < 0.01$, $***P < 0.001$.

Supplementary Material

Refer to Web version on PubMed Central for supplementary material.

Acknowledgments

This research was funded by the Howard Hughes Medical Institute. We thank J. Cox, A. Wardlaw, K. Morris for mouse breeding, genotyping, and viral injection support; S. Michael and A. Hu for histology support; M. Ramirez and B. Zemelman for rAAV production; and H. Gainer for discussions about the *Oxytocin* promoter; E. Boyden for technical assistance.

References

1. Cowley MA, et al. The distribution and mechanism of action of ghrelin in the CNS demonstrates a novel hypothalamic circuit regulating energy homeostasis. Neuron. 2003; 37:649–661. [PubMed: 12597862]
2. Andrews ZB, et al. UCP2 mediates ghrelin's action on NPY/AgRP neurons by lowering free radicals. Nature. 2008; 454:846–851. [PubMed: 18668043]
3. Yang Y, Atasoy D, Su HH, Sternson SM. Hunger states switch a flipflop memory circuit via a synaptic AMPK-dependent positive feedback loop. Cell. 2011; 146:992–1003. [PubMed: 21925320]

4. Aponte Y, Atasoy D, Sternson SM. AGRP neurons are sufficient to orchestrate feeding behavior rapidly and without training. Nat Neurosci. 2011; 14:351–355. [PubMed: 21209617]
5. Krashes MJ, et al. Rapid, reversible activation of AgRP neurons drives feeding behavior in mice. J Clin Invest. 2011; 121:1424–1428. [PubMed: 21364278]
6. Luquet S, Perez FA, Hnasko TS, Palmiter RD. NPY/AgRP neurons are essential for feeding in adult mice but can be ablated in neonates. Science. 2005; 310:683–685. [PubMed: 16254186]
7. Cannon, WB. The wisdom of the body. 2. W.W. Norton & Co; New York: 1939.
8. Broberger C, Johansen J, Johansson C, Schalling M, Hokfelt T. The neuropeptide Y/agouti gene-related protein (AGRP) brain circuitry in normal, anorectic, and monosodium glutamate-treated mice. Proc Natl Acad Sci U S A. 1998; 95:15043–15048. [PubMed: 9844012]
9. Gropp E, et al. Agouti-related peptide-expressing neurons are mandatory for feeding. Nat Neurosci. 2005; 8:1289–1291. [PubMed: 16158063]
10. Yaswen L, Diehl N, Brennan MB, Hochgeschwender U. Obesity in the mouse model of pro-opiomelanocortin deficiency responds to peripheral melanocortin. Nat Med. 1999; 5:1066–1070. [PubMed: 10470087]
11. Wu Q, Boyle MP, Palmiter RD. Loss of GABAergic signaling by AgRP neurons to the parabrachial nucleus leads to starvation. Cell. 2009; 137:1225–1234. [PubMed: 19563755]
12. Wu Q, Clark MS, Palmiter RD. Deciphering a neuronal circuit that mediates appetite. Nature. 2012; 483:594–597. [PubMed: 22419158]
13. Leibowitz SF, Hammer NJ, Chang K. Hypothalamic paraventricular nucleus lesions produce overeating and obesity in the rat. Physiol Behav. 1981; 27:1031–1040. [PubMed: 7335803]
14. Balthasar N, et al. Divergence of melanocortin pathways in the control of food intake and energy expenditure. Cell. 2005; 123:493–505. [PubMed: 16269339]
15. Xi D, Gandhi N, Lai M, Kublaoui BM. Ablation of Sim1 Neurons Causes Obesity through Hyperphagia and Reduced Energy Expenditure. PLoS One. 2012; 7:e36453. [PubMed: 22558467]
16. Avery L, Wasserman S. Ordering gene function: the interpretation of epistasis in regulatory hierarchies. Trends Genet. 1992; 8:312–316. [PubMed: 1365397]
17. Collins SR, et al. Functional dissection of protein complexes involved in yeast chromosome biology using a genetic interaction map. Nature. 2007; 446:806–810. [PubMed: 17314980]
18. Cowley MA, et al. Leptin activates anorexigenic POMC neurons through a neural network in the arcuate nucleus. Nature. 2001; 411:480–484. [PubMed: 11373681]
19. Tong Q, Ye CP, Jones JE, Elmquist JK, Lowell BB. Synaptic release of GABA by AgRP neurons is required for normal regulation of energy balance. Nat Neurosci. 2008; 11:998–1000. [PubMed: 19160495]
20. Petreanu L, Huber D, Sobczyk A, Svoboda K. Channelrhodopsin-2-assisted circuit mapping of long-range callosal projections. Nat Neurosci. 2007; 10:663–668. [PubMed: 17435752]
21. Boyden ES, Zhang F, Bamberg E, Nagel G, Deisseroth K. Millisecond-timescale, genetically targeted optical control of neural activity. Nat Neurosci. 2005; 8:1263–1268. [PubMed: 16116447]
22. Atasoy D, Aponte Y, Su HH, Sternson SM. A FLEX switch targets Channelrhodopsin-2 to multiple cell types for imaging and long-range circuit mapping. J Neurosci. 2008; 28:7025–7030. [PubMed: 18614669]
23. Dicken MS, Tooker RE, Hentges ST. Regulation of GABA and Glutamate Release from Proopiomelanocortin Neuron Terminals in Intact Hypothalamic Networks. J Neurosci. 2012; 32:4042–4048. [PubMed: 22442070]
24. Armbruster BN, Li X, Pausch MH, Herlitze S, Roth BL. Evolving the lock to fit the key to create a family of G protein-coupled receptors potently activated by an inert ligand. Proc Natl Acad Sci U S A. 2007; 104:5163–5168. [PubMed: 17360345]
25. Higgs S, Cooper SJ. Hyperphagia induced by direct administration of midazolam into the parabrachial nucleus of the rat. Eur J Pharmacol. 1996; 313:1–9. [PubMed: 8905322]
26. Hefft S, Jonas P. Asynchronous GABA release generates long-lasting inhibition at a hippocampal interneuron-principal neuron synapse. Nat Neurosci. 2005; 8:1319–1328. [PubMed: 16158066]
27. Best AR, Regehr WG. Inhibitory regulation of electrically coupled neurons in the inferior olive is mediated by asynchronous release of GABA. Neuron. 2009; 62:555–565. [PubMed: 19477156]

28. Kelly J, Rothstein J, Grossman SP. GABA and hypothalamic feeding systems. I Topographic analysis of the effects of microinjections of muscimol. Physiol Behav. 1979; 23:1123–1134. [PubMed: 542523]
29. Kublaoui BM, Gemelli T, Tolson KP, Wang Y, Zinn AR. Oxytocin deficiency mediates hyperphagic obesity of Sim1 haploinsufficient mice. Mol Endocrinol. 2008; 22:1723–1734. [PubMed: 18451093]
30. Magnus CJ, et al. Chemical and genetic engineering of selective ion channel-ligand interactions. Science. 2011; 333:1292–1296. [PubMed: 21885782]
31. Hodos W. Progressive ratio as a measure of reward strength. Science. 1961; 134:943–944. [PubMed: 13714876]
32. Swanson LW, Sawchenko PE. Hypothalamic integration: organization of the paraventricular and supraoptic nuclei. Annu Rev Neurosci. 1983; 6:269–324. [PubMed: 6132586]
33. Biag J, et al. Cyto- and chemoarchitecture of the hypothalamic paraventricular nucleus in the C57BL/6J male mouse: A study of immunostaining and multiple fluorescent tract tracing. J Comp Neurol. 2012; 520:6–33. [PubMed: 21674499]
34. Swaab DF, Purba JS, Hofman MA. Alterations in the hypothalamic paraventricular nucleus and its oxytocin neurons (putative satiety cells) in Prader-Willi syndrome: a study of five cases. J Clin Endocrinol Metab. 1995; 80:573–579. [PubMed: 7852523]
35. Holder JL Jr, Butte NF, Zinn AR. Profound obesity associated with a balanced translocation that disrupts the SIM1 gene. Hum Mol Genet. 2000; 9:101–108. [PubMed: 10587584]
36. Traurig M, et al. Common variation in SIM1 is reproducibly associated with BMI in Pima Indians. Diabetes. 2009; 58:1682–1689. [PubMed: 19401419]
37. Fields RL, Ponzio TA, Kawasaki M, Gainer H. Cell-type specific oxytocin gene expression from AAV delivered promoter deletion constructs into the rat supraoptic nucleus in vivo. PLoS One. 2012; 7:e32085. [PubMed: 22363799]
38. Knobloch HS, et al. Evoked axonal oxytocin release in the central amygdala attenuates fear response. Neuron. 2012; 73:553–566. [PubMed: 22325206]
39. Clark JT, Kalra PS, Crowley WR, Kalra SP. Neuropeptide Y and human pancreatic polypeptide stimulate feeding behavior in rats. Endocrinology. 1984; 115:427–429. [PubMed: 6547387]
40. Arletti R, Benelli A, Bertolini A. Oxytocin inhibits food and fluid intake in rats. Physiol Behav. 1990; 48:825–830. [PubMed: 2087513]
41. Swanson LW, Sawchenko PE, Wiegand SJ, Price JL. Separate neurons in the paraventricular nucleus project to the median eminence and to the medulla or spinal cord. Brain Res. 1980; 198:190–195. [PubMed: 7407584]
42. Blevins JE, Eakin TJ, Murphy JA, Schwartz MW, Baskin DG. Oxytocin innervation of caudal brainstem nuclei activated by cholecystokinin. Brain Res. 2003; 993:30–41. [PubMed: 14642828]
43. Zhang G, et al. Neuropeptide exocytosis involving synaptotagmin-4 and oxytocin in hypothalamic programming of body weight and energy balance. Neuron. 2011; 69:523–535. [PubMed: 21315262]
44. Baskin DG, et al. A new oxytocin-saporin cytotoxin for lesioning oxytocin-receptive neurons in the rat hindbrain. Endocrinology. 2010; 151:4207–4213. [PubMed: 20610562]
45. Kaelin CB, Xu AW, Lu XY, Barsh GS. Transcriptional regulation of agouti-related protein (Agrp) in transgenic mice. Endocrinology. 2004; 145:5798–5806. [PubMed: 15345681]
46. Balthasar N, et al. Leptin receptor signaling in POMC neurons is required for normal body weight homeostasis. Neuron. 2004; 42:983–991. [PubMed: 15207242]
47. Young WS 3rd, et al. Transgenic expression of green fluorescent protein in mouse oxytocin neurones. J Neuroendocrinol. 1999; 11:935–939. [PubMed: 10583728]
48. Pinto S, et al. Rapid rewiring of arcuate nucleus feeding circuits by leptin. Science. 2004; 304:110–115. [PubMed: 15064421]
49. Erickson JC, Clegg KE, Palmiter RD. Sensitivity to leptin and susceptibility to seizures of mice lacking neuropeptide Y. Nature. 1996; 381:415–421. [PubMed: 8632796]

50. Aravanis AM, et al. An optical neural interface: in vivo control of rodent motor cortex with integrated fiberoptic and optogenetic technology. J Neural Eng. 2007; 4:S143–156. [PubMed: 17873414]

51. Wieland HA, Engel W, Eberlein W, Rudolf K, Doods HN. Subtype selectivity of the novel nonpeptide neuropeptide Y Y1 receptor antagonist BIBO 3304 and its effect on feeding in rodents. Br J Pharmacol. 1998; 125:549–555. [PubMed: 9806339]

52. Zhang M, Balmadrid C, Kelley AE. Nucleus accumbens opioid, GABaergic, and dopaminergic modulation of palatable food motivation: contrasting effects revealed by a progressive ratio study in the rat. Behav Neurosci. 2003; 117:202–211. [PubMed: 12708516]

53. Peng H, Ruan Z, Atasoy D, Sternson S. Automatic reconstruction of 3D neuron structures using a graph-augmented deformable model. Bioinformatics. 2010; 26:i38–46. [PubMed: 20529931]

54. Sohn JW, et al. Serotonin 2C receptor activates a distinct population of arcuate pro-opiomelanocortin neurons via TRPC channels. Neuron. 2011; 71:488–497. [PubMed: 21835345]

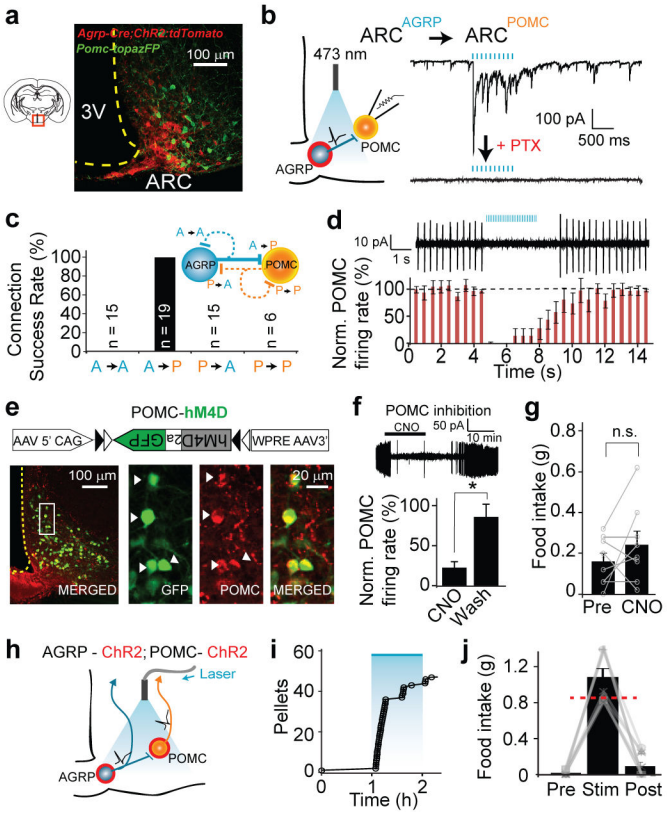

Figure 1. ARC^{AGRP}→ARC^{POMC} is not required for evoked feeding

a, ARC in *Agrp-Cre;Pomc-TopazFP* mice expressing ChR2:tdTomato in AGRP neurons. **b**, Left, scheme for testing ARC^{AGRP}→ARC^{POMC} synaptic connections. Red: ChR2:tdTomato. Right, ARC^{AGRP}→ARC^{POMC} synaptic currents. Blue: light pulses. **c**, Synaptic connectivity between AGRP and POMC neurons. Dashed lines: not detected. **d**, Cell-attached recording (top) and normalised firing rate (bottom, $n = 5$) from ARC^{AGRP}→ARC^{POMC} photostimulation in brain slices (with Npy1r, Npy5r, and $GABA_B$ receptor antagonists). **e**, POMC neuron expression of hM4D and GFP from Cre-dependent rAAV. **f**, Top, hM4D agonism with CNO (10 μM). Bottom, firing rate normalised to baseline (paired *t*-test, $n = 4$). **g**, Intraperitoneal CNO (5 mg/kg) did not increase food intake (1 h) in POMC-hM4D mice (paired *t*-test, $P = 0.32$, $n = 8$). **h–j**, Occlusion of ARC^{AGRP}→ ARC^{POMC} inhibition by optical co-stimulation of AGRP and POMC neurons (**h**) did not impair the feeding response (**i**,**j**) ($n = 9$). Pre, Stim, Post: before, during (blue), after photostimulation (1 h each). Red line: AGRP neuron-evoked food intake from ref. 4. Values are means ± s.e.m. n.s.: not significant, $^*P < 0.05$.

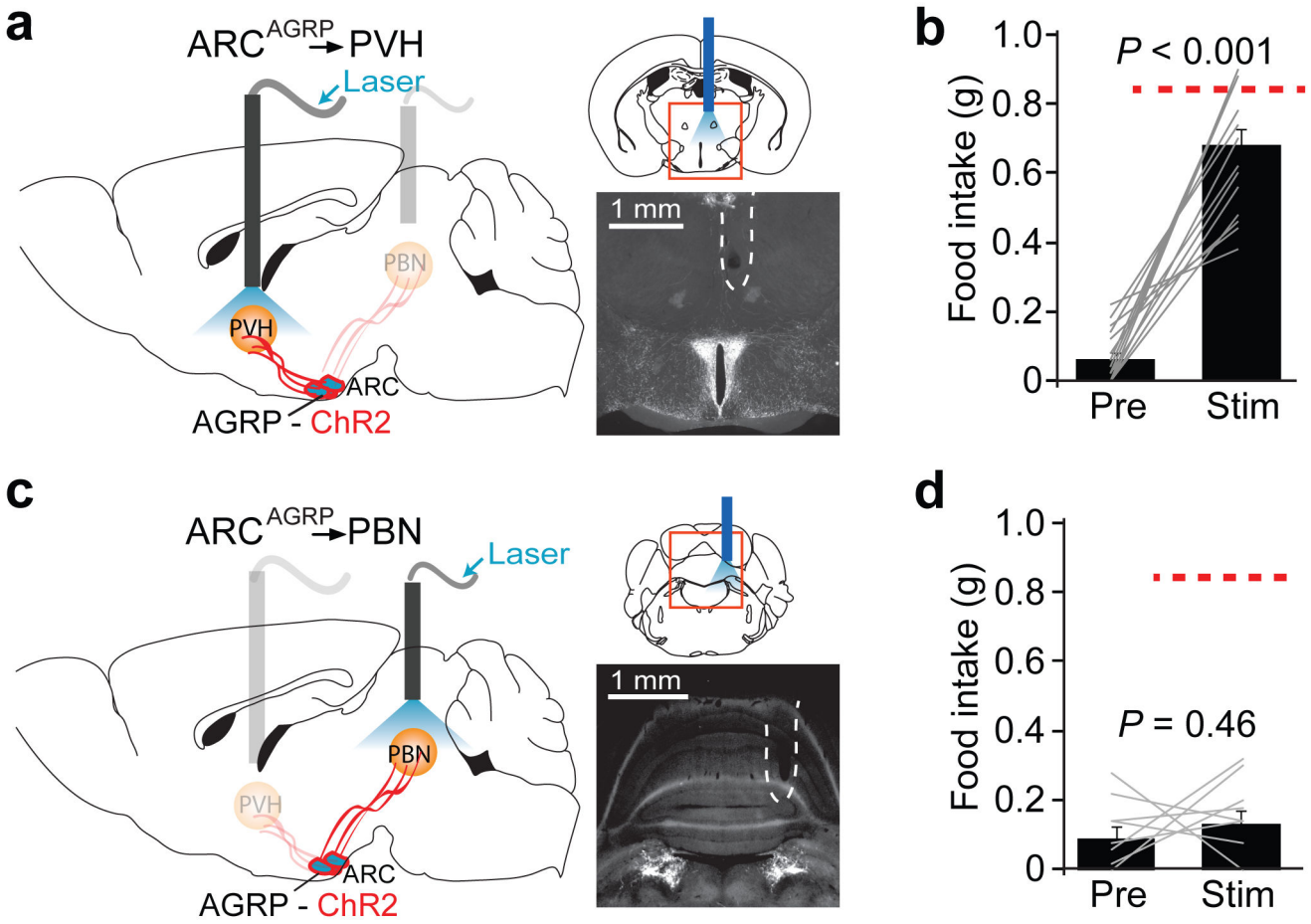

Figure 2. AGRP axon stimulation evokes feeding in PVH but not PBN

a, Scheme for AGRP axon photostimulation in the PVH and ChR2:tdTomato distribution of bilaterally transduced AGRP axons in the PVH. Dashed line: optical fibre position. **b**, Food intake before and during photostimulation (1 h each) of AGRP axons in the PVH (n = 16 mice, 8 bilateral and 8 unilateral ChR2 transduction). Red line: somatic AGRP neuron-evoked food intake (ref. 4). **c**,**d**, Photostimulation of AGRP axons with a second optical fibre implanted over the PBN (the bilaterally transduced mice used in **b**). Paired t-test. Values are means ± s.e.m.

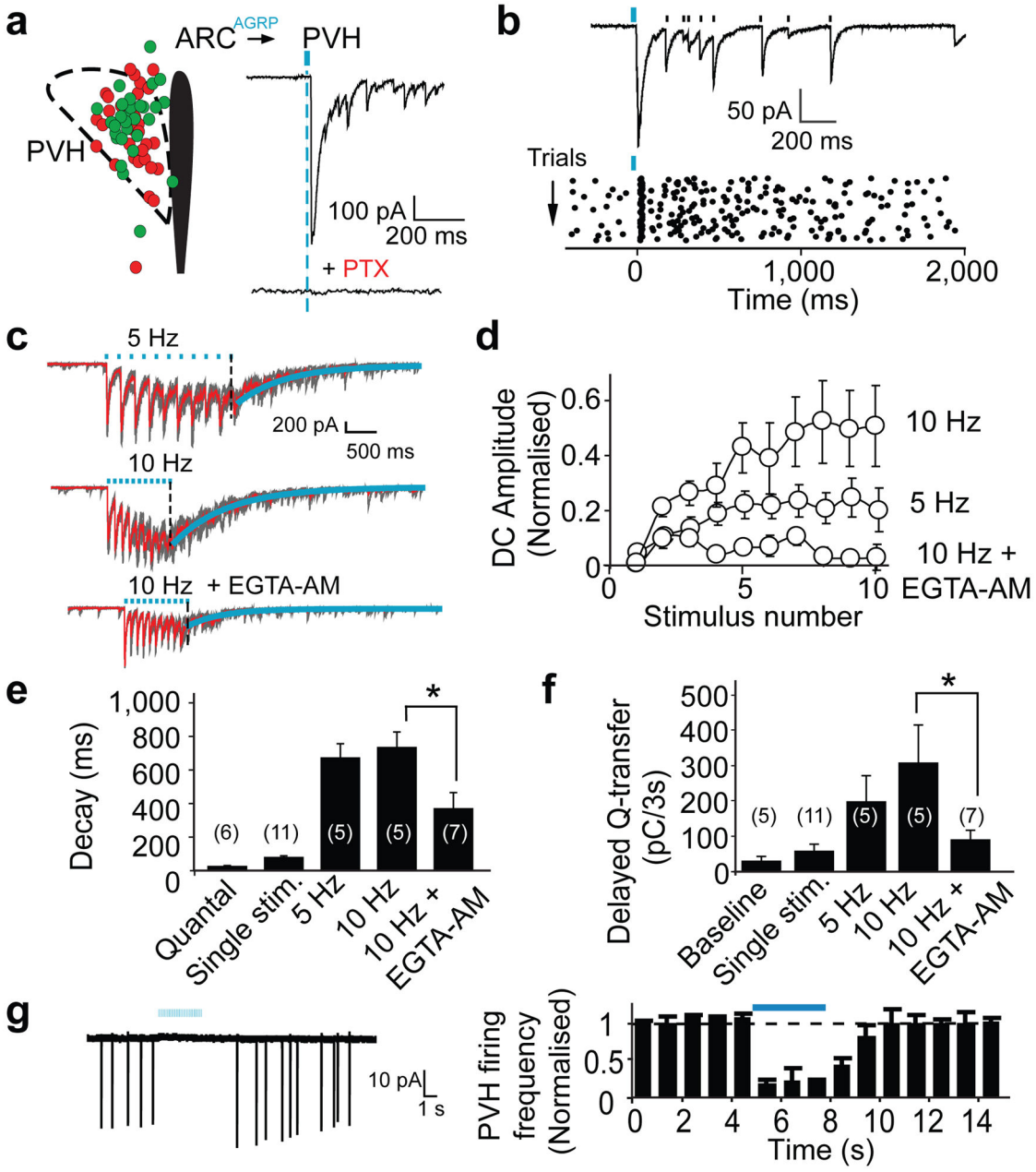

Figure 3. Prolonged ARC^{AGRP}→PVH synaptic inhibition

a, Distribution of ARC^{AGRP}→PVH postsynaptic neurons. Green: synaptic current detected, red: not detected. Blue tick: light pulse. **b**, Representative ARC^{AGRP}→PVH IPSC (above); raster plot of IPSCs (below). **c**, ARC^{AGRP}→PVH repetitive photostimulation. Gray: trials, red: average, blue: post-stimulus exponential fit. **d**, Normalised DC amplitude (see Methods). **e**,**f** Post-stimulus delayed release: decay time constant (**e**) and cumulative charge transfer (**f**) (sample sizes in parentheses, unpaired *t*-test). **g**, Left, PVH neuron silenced by AGRP axon photostimulation (10 Hz, with Npy1r, Npy5r, and $GABA_B$ receptor

antagonists). Right, normalised average firing rates (n = 9). Values are means ± s.e.m. *P < 0.05.

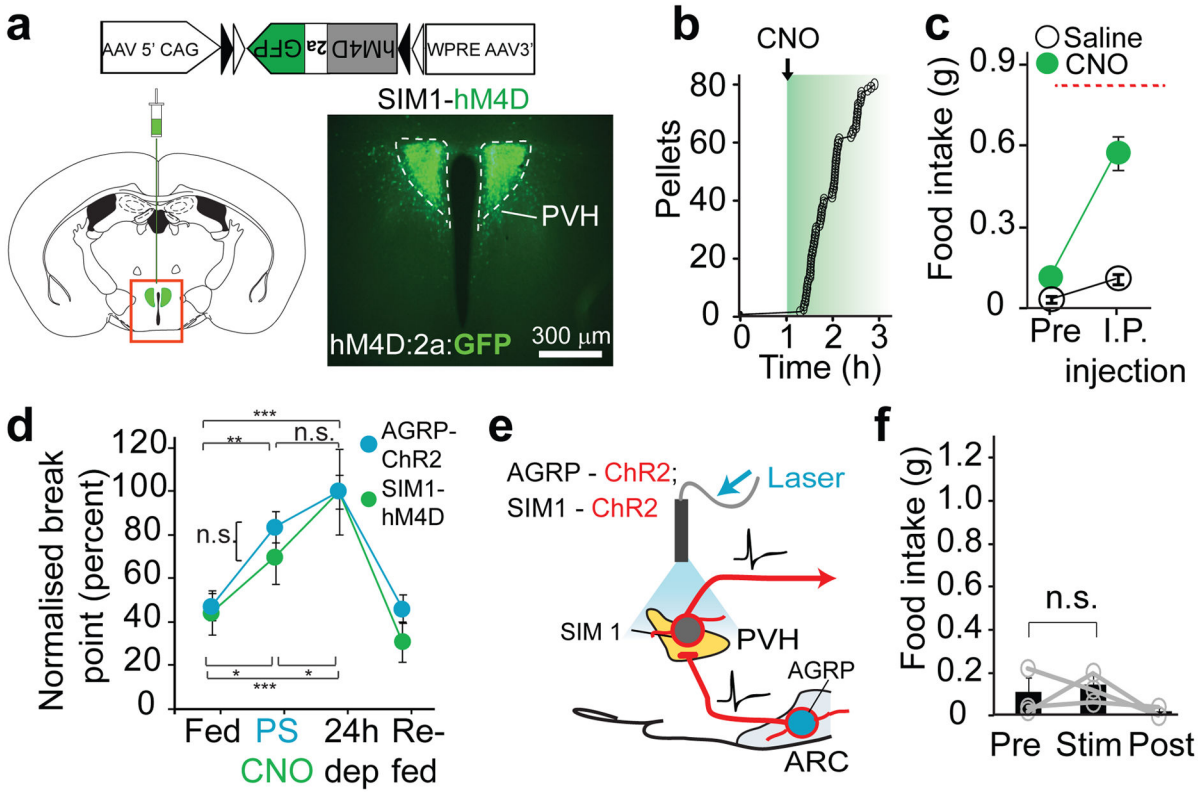

Figure 4. PVH neuron inhibition recapitulates feeding from AGRP neuron activation

a, Cre-dependent rAAV expression of hM4D and GFP in PVH SIM1 neurons. **b**, Food intake before and after intraperitoneal CNO (5 mg/kg) in SIM1-hM4D mouse. **c**, Food intake before and after CNO (n = 19) or saline (n = 9). Red line: AGRP neuron-evoked feeding (ref. 4). **d**, Normalised break point for AGRP-ChR2 (n = 6) or SIM1-hM4D (n = 6) mice (2-way ANOVA/1-factor repetition, condition: $F_{2,20}$ = 25.5, P <0.001; AGRP/SIM1: $F_{1,20}$ = 0.171, P = 0.69; interaction: $F_{2,20}$ = 0.45, P = 0.64; Holm-Sidak correction for multiple comparisons). Normalised to food deprivation (dep) break point. **e**, Scheme for co-photostimulation of AGRP axons and SIM1 neurons over the PVH, and (**f**) evoked food intake before, during, and after (1 h each) co-stimulation (paired t-test, n = 3). Values are means ± s.e.m. n.s.: not significant, *P < 0.05, **P < 0.01, ***P < 0.001.

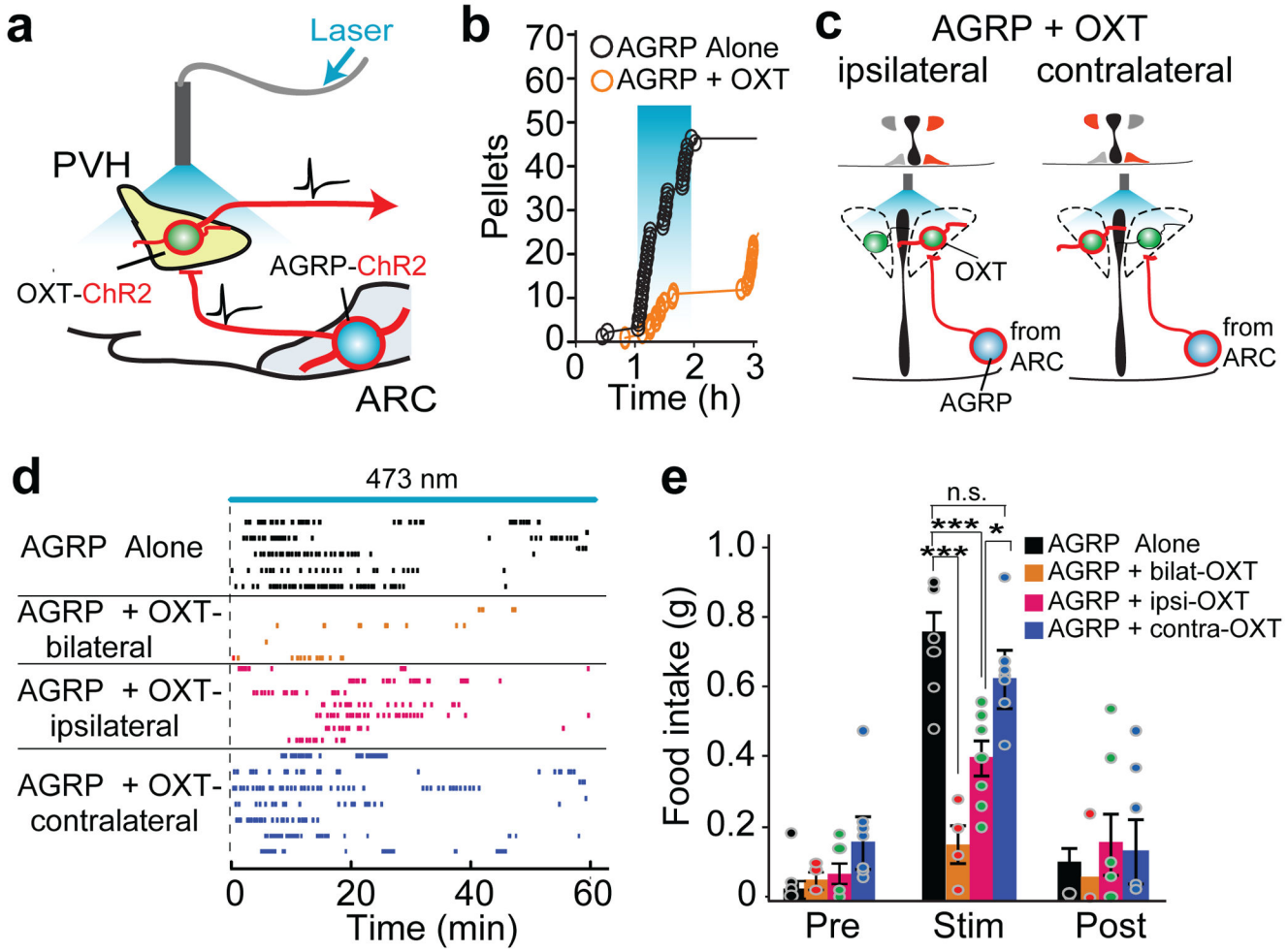

Figure 5. ARC^{AGRP}→PVH^{OXT} circuit contributes to evoked food intake

a,**b**, Co-photostimulation scheme for OXT neurons and AGRP axons over the PVH and (**b**) evoked food intake. Blue shading: photostimulation. **c**, Disconnection scheme for ARC^{AGRP}→PVH^{OXT}. **d**, Raster plot showing food pellets taken; rows: separate mice. **e**, Food intake before, during, and after photostimulation (1 h each). Within photostimulation condition: ANOVA, $F_{3,22} = 18.2$, $P < 0.001$; Holm-Sidak correction for multiple comparisons. Values are means ± s.e.m. n.s.: not significant, *$P < 0.05$, ***$P < 0.001$.

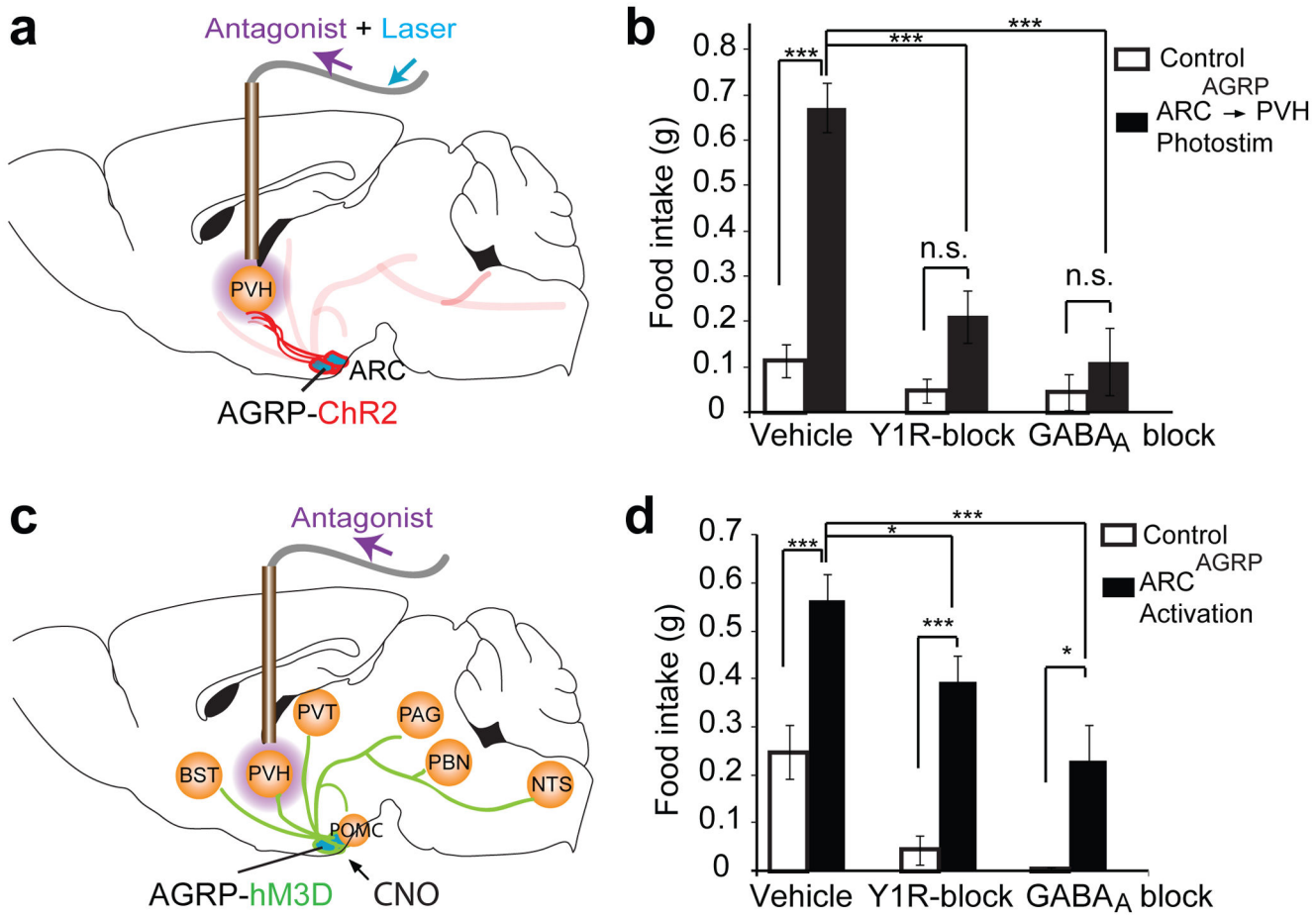

Figure 6. Pharmacological dissection of AGRP neuron-evoked feeding

a, Scheme depicting infusion of antagonists (purple) for $GABA_A$ receptors or Npy1r into the PVH followed by $ARC^{AGRP}\rightarrow$PVH axon photostimulation. **b,** Food intake during photostimulation (1 h) in ChR2-expressing mice (black, $n = 5$) and ChR2-negative mice (open bars, $n = 5$). 2-way ANOVA/1-factor repetition; $ARC^{AGRP}\rightarrow$PVH activation: $F_{1,16} = 24.4$, $P = 0.001$; antagonist: $F_{2,16} = 13.0$, $P < 0.001$; interaction: $F_{2,16} = 8.6$, $P = 0.003$. **c**, As in **a** except with somatic AGRP neuron activation using hM3D and CNO (0.3 mg/kg). **d**, Food intake (1 h) after intraperitoneal CNO injection in hM3D-expressing (black, $n = 8$) and non-transduced control mice (open bars, $n = 5$). 2-way ANOVA/1-factor repetition; neuron activation: $F_{1,20} = 22.8$, $P < 0.001$; antagonist: $F_{2,20} = 14.5$, $P < 0.001$; interaction: $F_{2,20} = 0.37$, $P = 0.694$. Holm-Sidak correction for multiple comparisons. Values are means ± s.e.m. n.s.: not significant,*$P < 0.05$, ***$P < 0.001$